$25p$

A STUDY OF LAUNCH-VEHICLE RESPONSES TO DETAILED

CHARACTERISTICS OF THE WIND PROFILE

☐ Conf.

By Harold C. Lester and Harold B. Tolefson [1964] 25p refs

16088751

NASA Langley Research Center,
Langley Station, Hampton, Va.

Presented at the { Fifth

AMS Fifth Conference on Applied Meteorology;
Atmospheric Problems of Aerospace Vehicles

GPO PRICE $ _____

CFSTI PRICE(S) $ _____

Hard copy (HC) ___/.00___

Microfiche (MF) ___.50___

ff 653 July 65

Atlantic City, New Jersey
March 2-6, 1964

A STUDY OF LAUNCH-VEHICLE RESPONSES TO DETAILED

CHARACTERISTICS OF THE WIND PROFILE

By Harold C. Lester[*] and Harold B. Tolefson[**]
NASA Langley Research Center

SUMMARY

35211

This paper examines the significance of the detailed variations in the vertical wind profile to launch-vehicle responses. Appreciable advances in the accuracy and the degree of detail obtainable in measurements of the winds experienced by vertically rising vehicles have been achieved by smoke-trail rocket sounding techniques and the wind measurements now available from these soundings are being applied to simulated in-flight loads studies. The analysis procedure and computer program employed in solving for the motions and bending moments experienced by a representative launch vehicle are discussed. The interaction of the vehicle's structure with the details of the wind profile is illustrated by a comparison of the structural bending moments with the features of the smoke-rocket measured profiles.

INTRODUCTION

Two important factors that must be considered in the design of a launch vehicle are the nature of the winds encountered during ascent through the atmosphere and the response of the vehicle to the winds. This cause and effect relationship between the wind inputs and the system response has been the subject of continuing study within the aerospace industry, but agreement has not been reached on an adequate representation of the wind disturbances or a satisfactory solution for the complete system responses to the winds. Evidence indicates, however, that the conventional balloon sounding which has provided the bulk of available wind measurements is not satisfactory for a complete examination of vehicle control requirements or a study of the attendant structural dynamics problems.

Both aspects of this problem, an accurate and detailed measurement of the winds and the calculation of the responses of flexible vehicles in traversing the winds, are considered in this paper. Application of the smoke-trail method as a means of obtaining high-resolution measurements of the vertical wind profile is discussed and sample measurements are used to illustrate pertinent features in the wind structure. An analysis procedure which has been developed to determine the motions and bending moments of a flexible vehicle flying through the detailed wind profiles is then outlined. The calculation procedure is applied to a typical launch vehicle to illustrate the interaction between the launch-vehicle structure and the details of the wind profile.

---

[*]Aerospace engineer, Dynamic Response Section, Dynamic Loads Division.
[**]Aerospace engineer, Structural Dynamics Branch, Dynamic Loads Division.

h   altitude, ft

L   length of launch vehicle, ft

M   Mach number, dimensionless

m_k propellant slosh mass, $lb\text{-}sec^2/ft$

q   dynamic pressure, $q = \frac{1}{2}\rho V_{mw}^2$, lb/ft^2

$q_i(t)$ generalized coordinate associated with the ith mode, ft

t   time, sec

$u(x,t)$ elastic displacement of structural center line, ft

V_m center-of-gravity velocity of launch vehicle, ft/sec

V_{mw} velocity of launch vehicle relative to the wind, ft/sec

V_w horizontal wind velocity, ft/sec

V_x, V_y components of the center-of-gravity velocity vector along the X and Y axes, respectively, ft/sec

X,Y   body-fixed coordinate axes

x,y   coordinates along X and Y body axes, ft

x_{cg} coordinate locating center of gravity, ft

x_k propellant slosh mass location, ft

$x_\theta, x_{\dot\theta}$ coordinates locating attitude and attitude rate sensors, respectively, ft

α rigid-body angle of attack, $\alpha = \tan^{-1}\left(\frac{-V_y}{V_x}\right)$, radians

α_w wind-induced angle of attack, radians

γ flight-path angle, $\gamma = \theta - \alpha$, radians

δ gimbal engine deflection angle, radians

δ_c gimbal engine command signal, radians

θ, θ_c attitude and attitude command angles, respectively, radians

θ_f feedback angle, radians

θ_e error angle, $\theta_e = \theta_c - \theta_f$, radians

λ_k propellant slosh coordinate as measured from the deformed structural
          center line, ft

ρ atmospheric density at altitude h, $lb\text{-}sec^2/ft^4$

$\phi_i(x)$ displacement of the ith mode, dimensionless

SMOKE-TRAIL WIND MEASUREMENTS

The smoke-trail method of measuring the details of the wind structure has
been described elsewhere (see refs. 1 to 3) and only a very brief review of the
technique will be given here. Essentially, a near-vertical filament of smoke
is laid by a small rocket to provide a sensitive tracer of the winds to alti-
tudes of near 65,000 feet. Time-lapse photographs from modified aerial mapping
cameras in operation at ground installations then provide a basis for calcu-
lating wind velocities from the trail displacements over given time intervals.
Some examples of these trails which are of particular interest to the present
wind measurement problem are given in figure 1.

Figure 1 shows three separate trails which were laid by a salvo of smoke
rockets launched at Wallops Island. The launchings were made to determine the
relative merits of three different chemicals for producing trails up to an
altitude of about 65,000 feet and the photograph shows the character of the
trails 60 seconds after rocket launching. A valuable byproduct of these tests
of interest to this paper is the three independent measurements of the wind
profile taken at the same time, but separated laterally by distances up to
$1\frac{1}{2}$ miles. Radar trackings of the three rockets indicated that the two trails
on the right of the figure were initially separated by about 1/4 to 1/2 mile,
and the two outermost trails were separated by about $1\frac{1}{2}$ miles.

The point of interest in figure 1 is the similarity between the three
smoke trails. A close examination of the sequence of photographs from which
figure 1 was taken indicates that the trails are almost exact images of one
another down to a high degree of detail and for the several minutes of time
covered by the sequence of pictures. These results give graphic evidence that
the characteristics of the wind-flow field were very consistent within the
region sampled for this case, and that under some circumstances the spatial
wind variations may be quite small.

The three wind profiles deduced from time-lapse photographs of the trails shown in figure 1 are given in figure 2. For the purpose of this paper, the vector winds are given in figure 2 and in similar plots that follow. Only minor differences can be detected in the three vertical wind profiles, thus confirming the observations made in regard to the consistency of the winds in figure 1. The wind profile identified as "B" in figure 2 extends only up to about 37,000 feet because the particular chemical used in this rocket failed to produce a visible trail at higher altitudes (see fig. 1).

The following table has been prepared to summarize the root-mean-square differences between the wind profiles A, B, and C of figure 2.

RMS vector wind-velocity difference (fps) as a function of altitude				
Trails	Altitude interval on trail, ft			
	13,000 to 23,000	23,000 to 31,000	31,000 to 37,000	37,000 to 50,000
A-B	1.5	2.7	1.4	---
B-C	1.6	3.1	1.1	---
A-C	1.4	2.0	1.2	1.9

Note that the RMS vector wind-velocity differences are less than about 1.5 fps for the lower and upper portions of the profiles and less than 2.5 or 3.0 fps for the midregion of relatively large shear. Previous studies (see ref. 1, for example) have indicated that the RMS wind measurement errors for the Wallops installation might be of the order of 0.5 fps. Application of this value to the preceding table would leave a residual of about 2 fps or less as the wind-velocity variations within the area represented by the three profiles of figure 2.

The profile identified as "C" in figure 2 will be used later in this paper as an input disturbance to a vertically rising launch vehicle to study responses to atmospheric winds. It is pertinent to note at this time that the winds for this case reach a peak velocity of 225 fps at an altitude near 30,000 feet, and that a rather severe shear layer is present below the jet stream level. The overall flow appears rather smooth with only a few small-scale disturbances present at altitudes above 35,000 feet.

Figure 3 shows the magnitude of the wind vector plotted against altitude for two additional Wallops smoke-trail measurements. The distinctive features of these profiles is the large shear layer which peaks at an altitude of 40,000 feet for profile D and the small-scale disturbances throughout profile E. Also no large shear reversal is present at the tropopause level for profile E. Thus, while the major vehicle response for profiles C and D might be expected

to result from the large shear reversal near 30,000 and 40,000 feet, respectively, the random small-scale disturbances of profile E may excite the predominate elastic modes of the vehicle throughout the altitude range covered by the profile.

Figure 4 shows two other smoke-trail wind profiles which illustrate the variable nature of the wind input. Profile G in figure 4 is of particular interest to this study since the peak wind speed of about 300 fps at 35,000 feet corresponds to the peak wind for the well-known 1-percent synthetic wind profile developed by the Air Force Cambridge Research Laboratories (ref. 4). The wind shear values immediately below and above the peak, however, are only one-half or less than the Air Force recommended value of 0.045 per second. The peculiar step arrangement in the wind velocities over the altitude range of 10,000 to 30,000 feet for profile G might be expected to induce appreciable responses in a vertically rising vehicle.

METHOD OF ANALYSIS

Computation of the response and flight loads experienced by a launch vehicle as it ascends through measured atmospheric winds requires a method of describing the vehicle to at least the same degree of refinement as achieved in the wind input data. Inasmuch as only the gross atmospheric wind motions can be deduced with any degree of certainty from conventional balloon soundings, it has been customary in the past to predict wind loads on the basis of a simplified representation of a launch vehicle as, for example, by using a rigid-body vehicle description. Loads obtained from rather arbitrary (1-cosine) shaped gusts acting on a flexible vehicle are then superimposed on the wind loads to yield a total load. Since detailed measurements provided by the smoke-trail method define the higher frequency disturbances as well as the large-scale motions of the wind field, it is necessary to describe a launch vehicle by an extended mathematical model which accounts, not only for the rigid motion, but also for the structural flexibility and propellant slosh.

Such an analytical procedure has been developed at the NASA Langley Research Center to predict launch-vehicle flight loads using smoke rocket wind profiles. Essential features of the method are summarized in the appendix. Briefly, the method considers the pitch plane motion, as shown in figure 5, of an ascending launch vehicle which is described mathematically by a set of non-linear differential equations with time-dependent coefficients. The rigid-body motion is described by translatory motion along body-fixed Cartesian axes and a pitching motion about the center of gravity. Bending of the vehicle's structure is approximated by a superposition of several free-free vibration modes, and simple spring-mass systems are used to represent propellant slosh. Control forces are produced by thrust vectoring.

The sample calculations presented in this paper were obtained by applying the method to a representative vehicle. The smoke-trail wind measurements given as profiles C through G in figures 2, 3, and 4 were used as wind input data. Pertinent features of the example launch vehicle were those of a large

liquid-propellant booster having a lift-off thrust-to-weight ratio of about 1.25. Aerodynamically, the vehicle is a cone cylinder with the cone length being about 15 percent of the total length and the diameter of the vehicle about 8.5 percent of the total length. Structurally, the vehicle was represented by the superposition of the first three free-free beam modes. The first mode frequency increased from about 2.0 cps at lift-off to about 2.5 cps after 90 seconds of flight. Two slosh degrees of freedom, representing the fundamental modes of the first-stage lox and fuel, were used. The vehicle was commanded to ascend vertically for the first 15 seconds of flight and then to execute a gradual pitch-over which approximated a zero-lift trajectory. References 5 and 6 contain additional information on the analysis method and the particular launch vehicle used for the sample calculations presented herein.

RESULTS AND DISCUSSION

In this section the bending moments and responses calculated for the example launch vehicle using wind profiles C through G are presented and discussed. It should be noted that the planar nature of the response equations place a similar restriction on the wind input data and, hence, the profiles shown reflect the altitude distribution of the magnitude of the resultant wind-velocity vector and therefore neglect the effects of wind direction. Wind profiles C through G represent wind motions from west to east and hence were utilized as tail winds in the computer program in order to simulate an easterly launching. In addition, the wind velocities were linearly extended from the lowest data point in each profile to zero velocity at the surface.

Trajectory Characteristics

Typical trajectory and loading parameter time histories are presented in figures 6 and 7 for flight of the vehicle through profile E (fig. 3). Dynamic pressure, Mach number, and altitude are shown in figure 6. For this particular wind profile the vehicle exhibits a peak value of dynamic pressure of about 740 lb/ft^2 at a flight time of approximately 78 seconds. Flight speed becomes supersonic at about 61 seconds after lift-off. The vectorial combination of the wind velocity with the inertial velocity of the vehicle is readily apparent in figure 6 in the dynamic pressure curve between 70 seconds and 85 seconds. The altitude curve indicates that the vehicle required about 85 seconds to fly to approximately 54,000 feet which corresponds to the terminal data point for this particular profile and is beyond the point of maximum dynamic pressure.

Time histories for the total angle of attack, pitch attitude, and gimbal angle, which may be regarded as load parameters, are illustrated in figure 7 for flight through profile E. As indicated by the attitude time history, the vehicle ascended vertically for the first 15 seconds of flight and then at an altitude of about 1,000 feet executed a slow pitch-over maneuver which approximates a zero-lift trajectory. The small values for the wind-induced oscillations in the pitch attitude indicate that very tight attitude control was maintained.

6

The angle-of-attack curve shows appreciable dependence on the wind input profile as can be noted by a comparison with figure 3. The measured wind profile was not actually entered until a flight time of about 42 seconds; after that time considerable fluctuations were induced in the angle of attack due to the random wind variations. A peak angle of attack of about -6° occurs early in the flight during pitch-over, but is not indicative of large loads because of the small value for $(\alpha + \alpha_w)q$, the product of total angle of attack and dynamic pressure, existing at that time. The lower values of angle of attack which occur later in the time history, say at a time of about 58 seconds, when the peak angle of attack was about -5° are more significant in view of the large dynamic pressure. The motion of the gimbaling engine required for maintaining control and executing the pitch-over maneuver under the disturbing influence of wind profile E is also shown in figure 7. A maximum gimbal angle of 3° was required.

Bending-Moment Responses

The remaining figures discussed in this paper show bending-moment and angle-of-attack time histories for smoke trails C through G. The longitudinal station at which the bending moments are computed is located about 30 percent of the total vehicle length forward of the gimbal station (thrust point) and is in close proximity to the station at which the maximum bending moment usually occurs.

Part (a) of figure 8 shows the time histories obtained with smoke profile C as input (see fig. 2). Comparison of the bending-moment curve with the angle-of-attack time history and the velocity profile C indicates that the loading follows the angle of attack, that is, peak loads coincide with peak angles of attack. The maximum bending moment of about 550,000 ft-lb occurs at approximately 61 seconds and is induced by the large shear layer of trail C between altitudes of about 22,000 feet and 27,000 feet. The maximum shear intensity and calculated bending moments are listed in table I for the different profiles. Several positive peak loads occur between 70 and 90 seconds in figure 8(a) due to the vehicle recovering from the large shear reversal and the smaller shear layers between 40,000 feet and 60,000 feet (see fig. 2). The first bending-mode responses of the present vehicle may be noted as the 2- to $2\frac{1}{2}$-cps oscillation superimposed on the bending-moment time histories of figure 8(a). In spite of the small-scale fluctuations at higher altitudes in trail C the structural response is not large and is probably excited, in part, by engine transients.

The upper part of figure 8(b) shows the resulting bending-moment and angle-of-attack responses for flight through trail D of figure 3. Again a large shear layer characterizes this wind profile, but the shear reversal occurs at a higher altitude, beginning at about 37,000 feet, than the similar reversal of trail C. Because of the peaking in dynamic pressure which occurs at about 80 seconds (44,000 ft) this wind profile would be expected to produce slightly larger loads than trail C. The bending-moment time history, however, indicates a maximum peak load of about 300,000 ft-lb at 76 seconds, a reduction which is proportional to the reduction in the peak shears between the two trails (see table I).

Again the response of the structure is not significant although the frequency of the first bending mode is clearly discernible in figure 8(b), especially at a time near 82 seconds. The bending-moment amplification in this case amounts to 8 or 10 percent, but due to the nature of the wind input, the major structural excitation occurred after maximum loading.

Trail E, as shown in figure 3, differs from the preceding trails in that it lacks the large shear layer that characterizes trails C and D. Here the wind buildup is more gradual and, as has been noted earlier, disturbances or gusts are superimposed throughout the height of the profile. Near 37,000 feet the trend is toward decreasing winds with increasing height.

The bending-moment time histories for smoke trail E are presented in the lower part of figure 8(b). Again the bending-moment response closely follows the angle of attack with a peak loading of about 480,000 ft-lb occurring at about 58 seconds of flight. The thin shear layer of intensity 0.020 sec^{-1} (see table I) accounts for this maximum loading condition. Coupling of the first mode is indicated especially around 48 seconds and later at about 80 seconds. The dynamic amplifications amount to about 30 percent at a time of 80 seconds and appear to result from the fluctuations in the wind profile near 40,000 feet. The overall bending moments, however, are relatively low at this point when compared to earlier portions of the flight.

The results obtained using wind profile F as input (fig. 4) are presented in figure 8(c). In general, the remarks made earlier concerning trails C and D seem applicable: The bending-moment response appears to be quasi-steady with angle of attack with little excitation of the structure. A peak bending moment of about ±300,000 ft-lb occurs between 75 seconds and 80 seconds with the associated angles of attack being about ±2°. The peak conditions are induced by the double shear layer between 35,000 feet and 40,000 feet.

Time histories for trail G (fig. 4) are also presented in figure 8(c). As was noted earlier, this profile has a very high peak wind velocity of about 300 fps. It also contains a large shear reversal between 30,000 feet and 40,000 feet and at the lower altitudes possesses several sudden almost step changes in velocity. As would be expected, these features of trail G dominate the bending-moment response which, again, is almost quasi-steady with angle of attack. A first-mode component is discernible, but is not large. Peak bending moments of about ±500,000 ft-lb occur between 70 and 80 seconds, respectively, and are induced by the vehicle recovering from the large shear reversal. Responses of the elastic modes account for about 3 percent of the maximum bending moment. The corresponding angles of attack for these peak loading conditions are about ±4°.

CONCLUDING REMARKS

A typical flexible-body launch vehicle has been flown through an ensemble of five detailed wind profiles in order to study interaction of the structure and control system with the wind structure. The wind profiles used were

8

measured at the NASA Wallops Station by the smoke-trail method. For the partic-ular launch vehicle used, the study revealed nominal bending-moment dynamic amplifications which might be expected to result from structural and control system coupling with the high-frequency content of the wind profiles. Some earlier studies as summarized in reference 3 had indicated the possibilities of substantially greater structural amplifications than found herein. The flight dynamic pressures for the solid-propellant vehicle considered in reference 3, however, were substantially greater than for the present vehicle. This factor together with larger amplitude wind fluctuations (but lower overall wind veloc-ities) led to significant percentage increases in peak loads. It becomes quite apparent that vehicles of different performance and structural characteristics should be examined separately for the expected wind environment.

APPENDIX

METHOD OF ANALYSIS

This appendix will be devoted to a brief discussion of the salient features of an analytical procedure developed to compute the response and bending loads experienced by a launch vehicle ascending through detailed atmospheric winds. Since space limitations prevent a rigorous derivation, a conceptual development, with reference to the literature, will be made. The appendix will conclude with a brief discussion of the computer program and numerical integration routine.

Coordinate System Considerations

Motion is constrained to the pitch plane and referenced to a body-fixed Cartesian coordinate system as shown in figure 5. The axes are fixed in the undeformed rigid body and are oriented to the local horizontal by the attitude angle θ. The rigid motion is characterized by translation along the respective body axes and a pitching motion about the center of gravity. Bending of the structure is approximated by the superposition of several free-free beam modes using the following series:

$$u(x,t) = \sum_i \phi_i(x) q_i(t)$$

The mode shapes $\phi_i(x)$ are functions of the mass and stiffness properties exhibited at discrete times in the trajectory and represent known input quantities. The generalized coordinates $q_i(t)$ determine the contribution of each mode and represent independent degrees of freedom. Liquid-propellant motion is approximated using several spring-mass systems. This analogy is developed in the literature for a variety of tank configurations. It duplicates the force exerted on a tank by the liquid when the fundamental slosh mode is excited at its resonant frequency. Control forces are produced by gimbaling the rocket engines through an angle δ in response to commands provided by an autopilot.

Aerodynamics

In the vector diagram of figure 5, the relationship between the various velocity vectors needed to define the aerodynamic forces is illustrated. The velocity vector of the center of gravity, for example, is oriented to the local horizontal by γ, the flight-path angle. The angle between the velocity component V_x of the center of gravity and the velocity of the vehicle relative to the wind V_{mw} defines the total angle of attack that the vehicle experiences. The horizontal wind-velocity component V_w is shown as a headwind.

Aerodynamic forces are assumed quasi-steady, based on normal-force distributions measured or calculated along the longitudinal axis. These forces are assumed linear with angle of attack and neglect the effect of the vehicle penetrating a gust front. Thus, the velocity vectors and angles of attack discussed previously and shown in figure 5 are defined at the launch vehicle's center of gravity. It should be noted also that the aerodynamic forces and moments are functions of Mach number, but are converted to functions of time for use in the computer program by a Mach number time relation from a nominal trajectory.

Derivation of the Equations of Motion

The equations of motion were derived using a variational principle founded on momentum concepts which yields Lagrange's equation as a special case. However, whereas the classical deviation of Lagrange's equations is based on the assumption of constant mass, no such limitation is imposed on the scaler equations of the variational method. The procedure is therefore applicable to variable mass systems. Details of the derivation and the resulting response equations are presented in the literature (refs. 5, 6, and 7).

Control System Considerations

The general description of a launch-vehicle control system is impractical because of the variety of types used. The autopilot discussed here and shown in block diagram form in figure 9 is that used by the example launch vehicle which was chosen to illustrate wind effects. A pitch-over program θ_c and a wind profile V_w serve as system inputs. The forward loop contains a signal-shaping network and the gimbaling engine is described by a third-order linear system with constant coefficients. Control system feedback is through two paths - an attitude channel and an attitude rate channel. The terms proportional to $q_i(t)$ represent the structural feedback. The control system and gimbal engine equations are summarized in the references cited previously. It should be noted that the solution of the response equations provides the ascent trajectory of the vehicle as it attempts to fly a specified pitch program under the disturbing effect of a detailed wind profile.
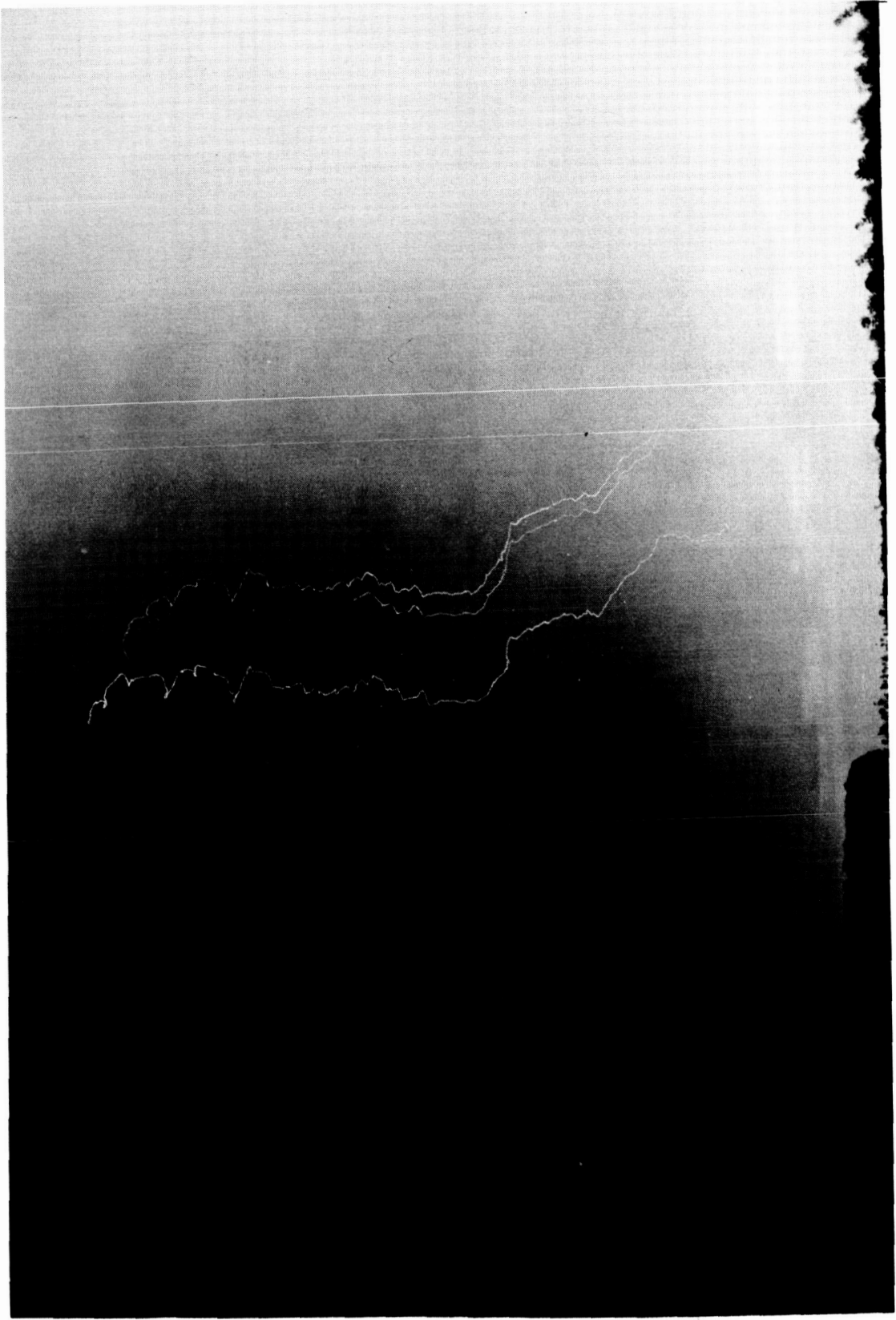
Computer Program

The launch-vehicle wind-response equation were programed for solution on a high-speed digital computer. Time-dependent input parameters were approximated using tabulated data and a linear interpolation subroutine. Atmospheric properties were obtained from a standard atmosphere. The equations were integrated by a fourth-order Runge-Kutta routine with a self-adjusting interval size and double-precision internal addition was used to reduce round-off error. Since the equations are linearly cross coupled through the acceleration, a matrix inversion was required to obtain the acceleration values.

REFERENCES

1. Tolefson, Harold B., and Henry, Robert M.: A Method of Obtaining Detailed Wind Shear Measurements for Application to Dynamic Response Problems of Missile Systems. Journal of Geophysics Research, Vol. 66, No. 9, Sept. 1961, pp. 2849-62.

2. Henry, Robert M., Brandon, George W., Tolefson, Harold B., and Lanford, Wade E.: The Smoke-Trail Method for Obtaining Detailed Measurements of the Vertical Wind Profile for Application to Missile-Dynamic-Response Problems. NASA TN D-976, 1961.

3. Tolefson, Harold B.: Smoke-Trail Measurements of the Vertical Wind Profile and Some Applications. Proceedings of the National Symposium on Winds for Aerospace Vehicle Design, Vol. I Air Force Surveys in Geophysics, No. 140, Mar. 1962, pp. 203-209.

4. Sissenwine, Norman: Windspeed Profile, Windshear, and Gusts for Design of Guidance Systems for Vertically Rising Air Vehicles. Air Force Surveys in Geophysics No. 57 (AFCRC TN-54-22), Nov. 1954.

5. Lester, Harold C., and Morgan, Homer G.: Determination of Launch Vehicle Response to Detailed Wind Profiles. Aerospace Sciences Meeting, New York, Jan. 20-22, 1964, Preprint No. 64-82.

6. Lester, Harold C., and Collins, Dennis F.: Determination of Loads on a Flexible Launch Vehicle During Ascent Through Winds. Proposed NASA TN.

7. Edelen, Dominig G. B.: On the Dynamical Effects of Fuel Flow on the Motion of Boost Vehicles. The Rand Corporation, Memorandum RM-3268 - NASA, October 1962.
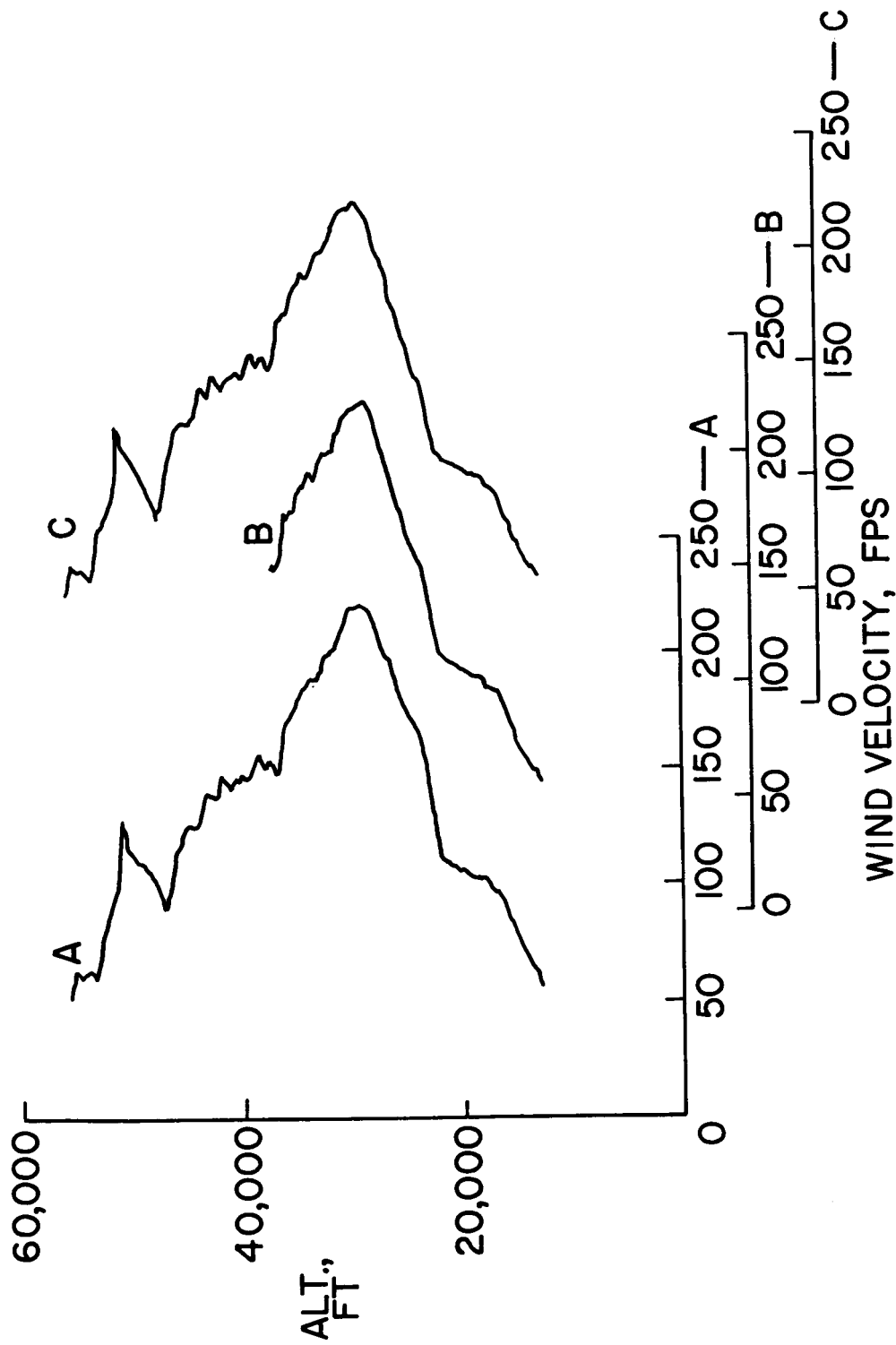
TABLE I.- MAXIMUM WIND SHEAR VALUES AND ASSOCIATED

VEHICLE BENDING MOMENTS

Trail	Time, sec	Approximate altitude range, thsds. ft	Wind shear, sec^{-1}	Calculated bending moment, ft-lb
C	64	22 to 27	0.021	-0.55×10^6
D	76	37 to 40	.013	-.30
E	58	19 to 20	.020	-.48
F	75	37 to 39	.027	.31
G	78	32 to 35	.017	.53

13

Figure 1.- Smoke rocket salvo.

NASA

Figure 2.- Simultaneous smoke-trail wind profile measurements.
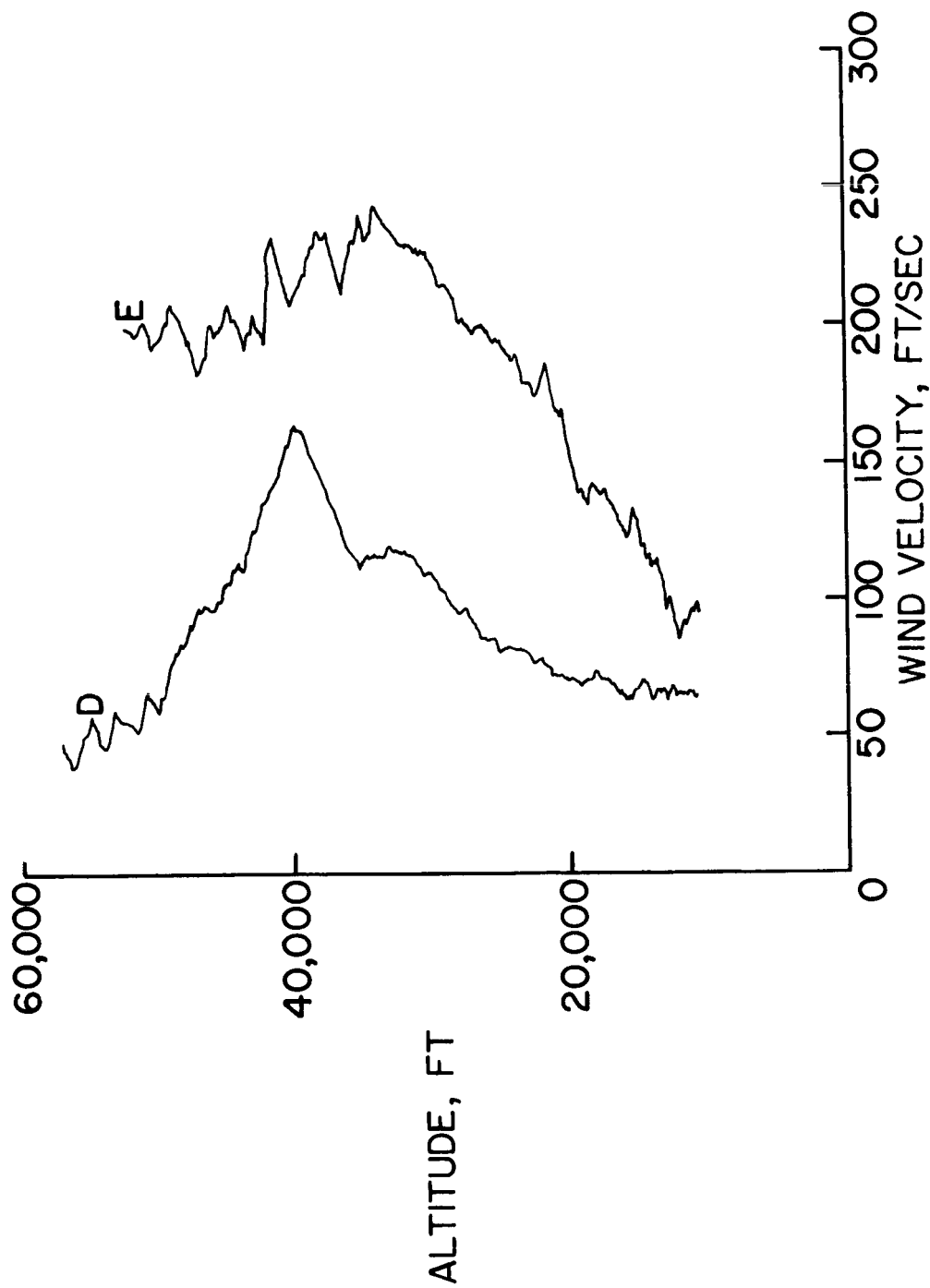
NASA

Figure 3.- Smoke-trail wind profile features.
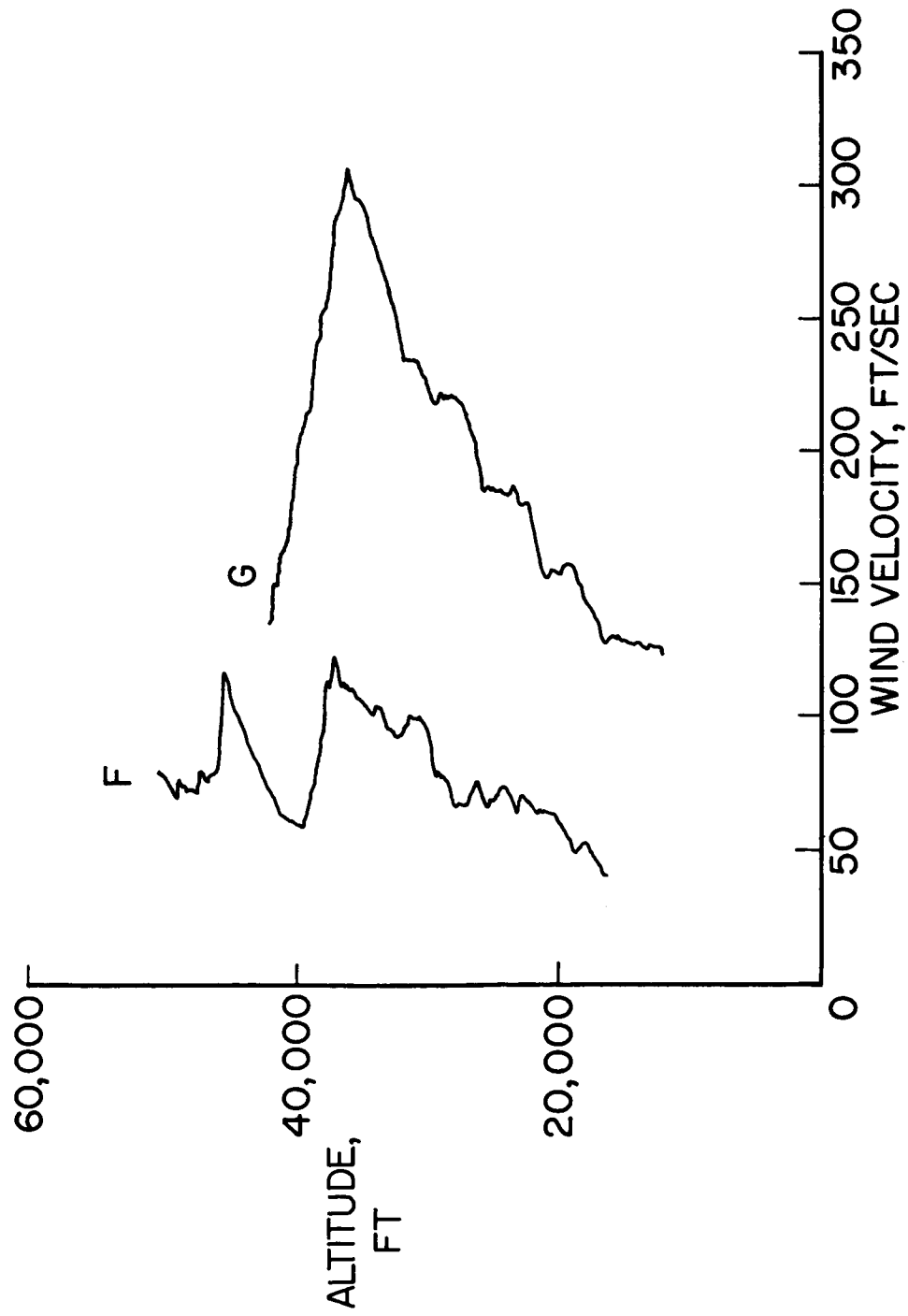
NASA

Figure 4.- Smoke-trail wind profile features.
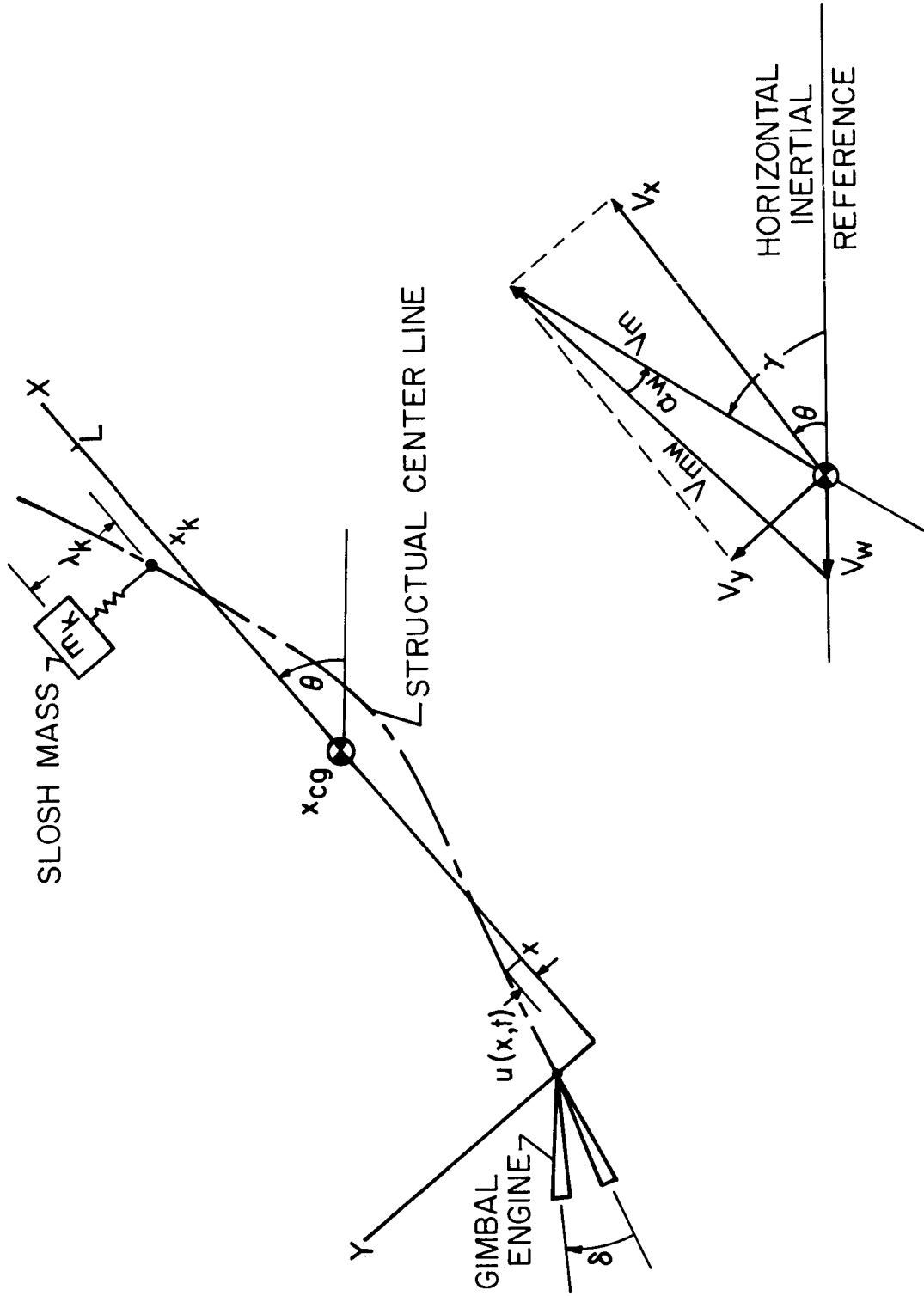
NASA

Figure 5.- Coordinate system.

NASA

q, LB/SQ FT

800

600

400

200

0

DYNAMIC
PRESSURE, q

MACH NUMBER, M

ALTITUDE, h

TIME, SEC

0   20   40   60   80   100

M
3

2

1

0

h, FT
80×10³

40

0
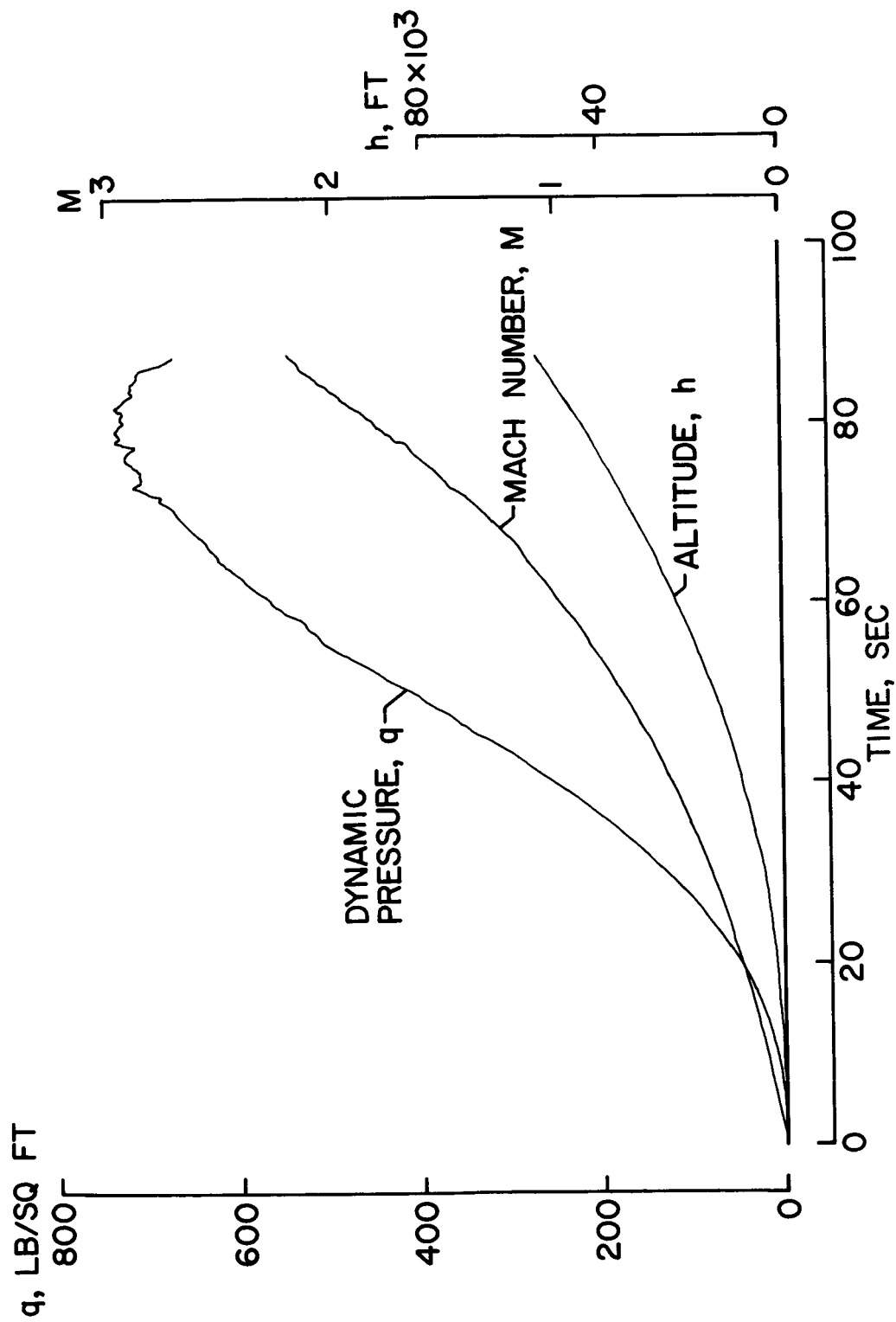
NASA

Figure 6.- Trajectory parameters.
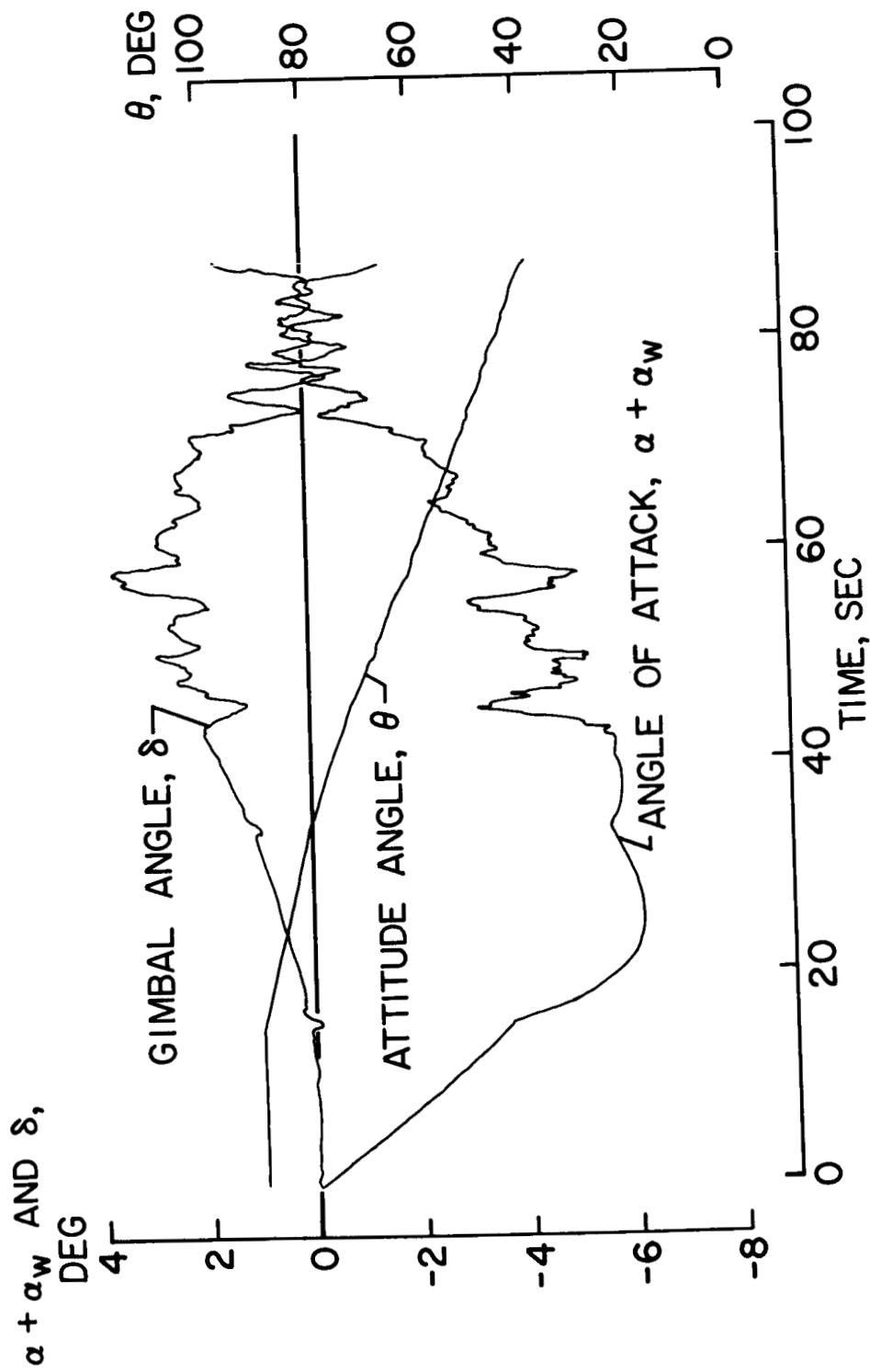
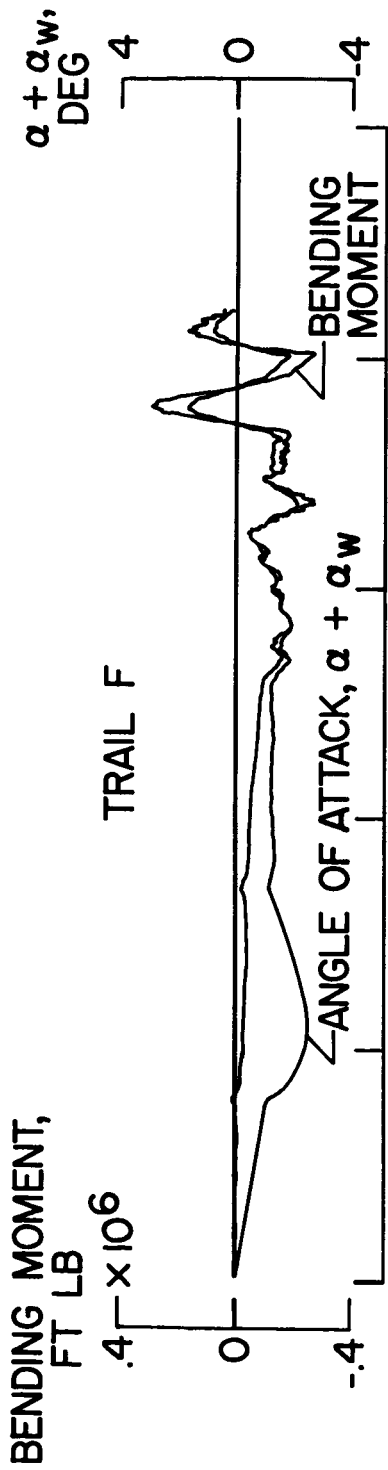Figure 7.- Loading parameters.
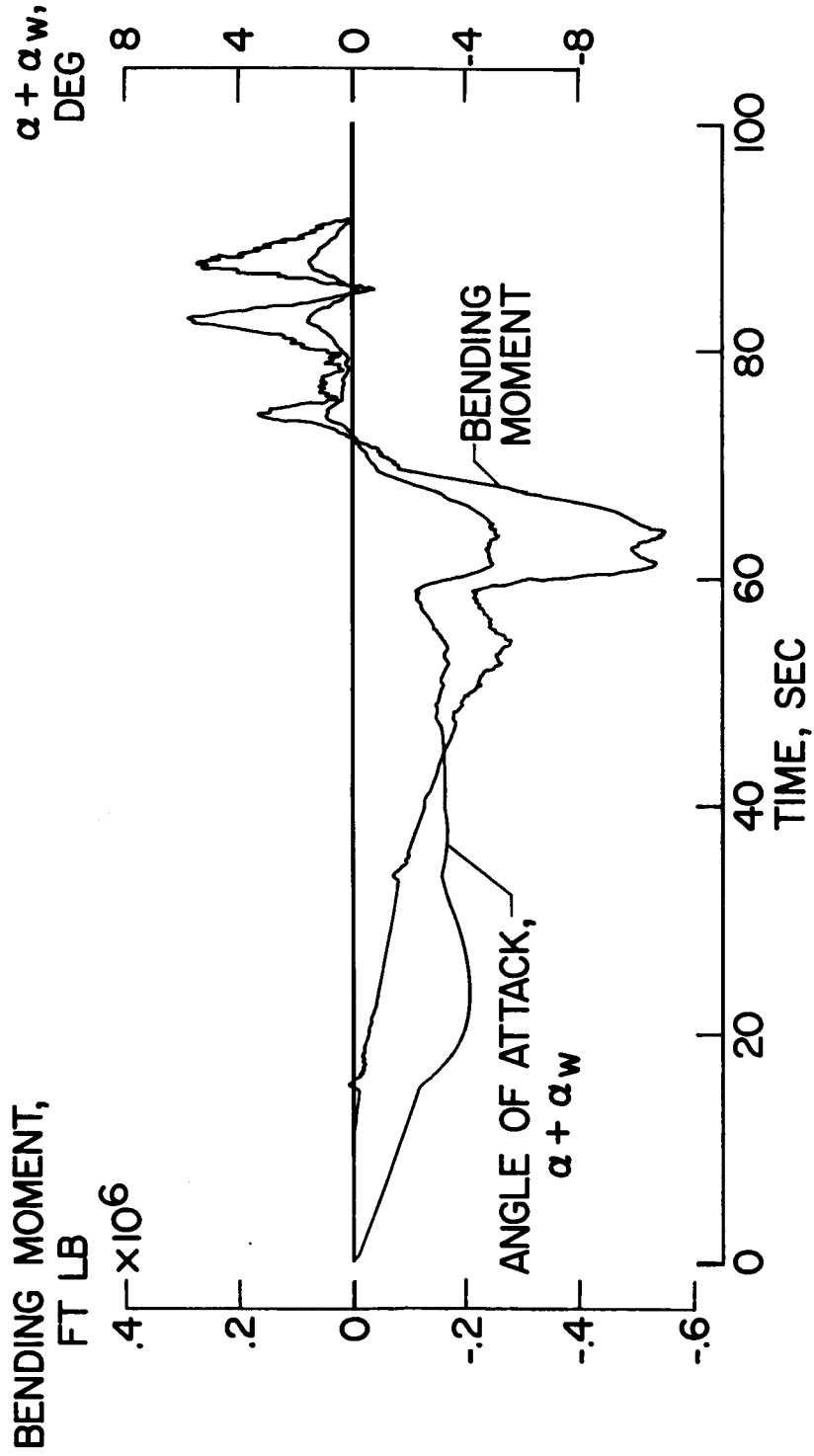
NASA

(a) Trail C.

Figure 8.- Calculated responses.
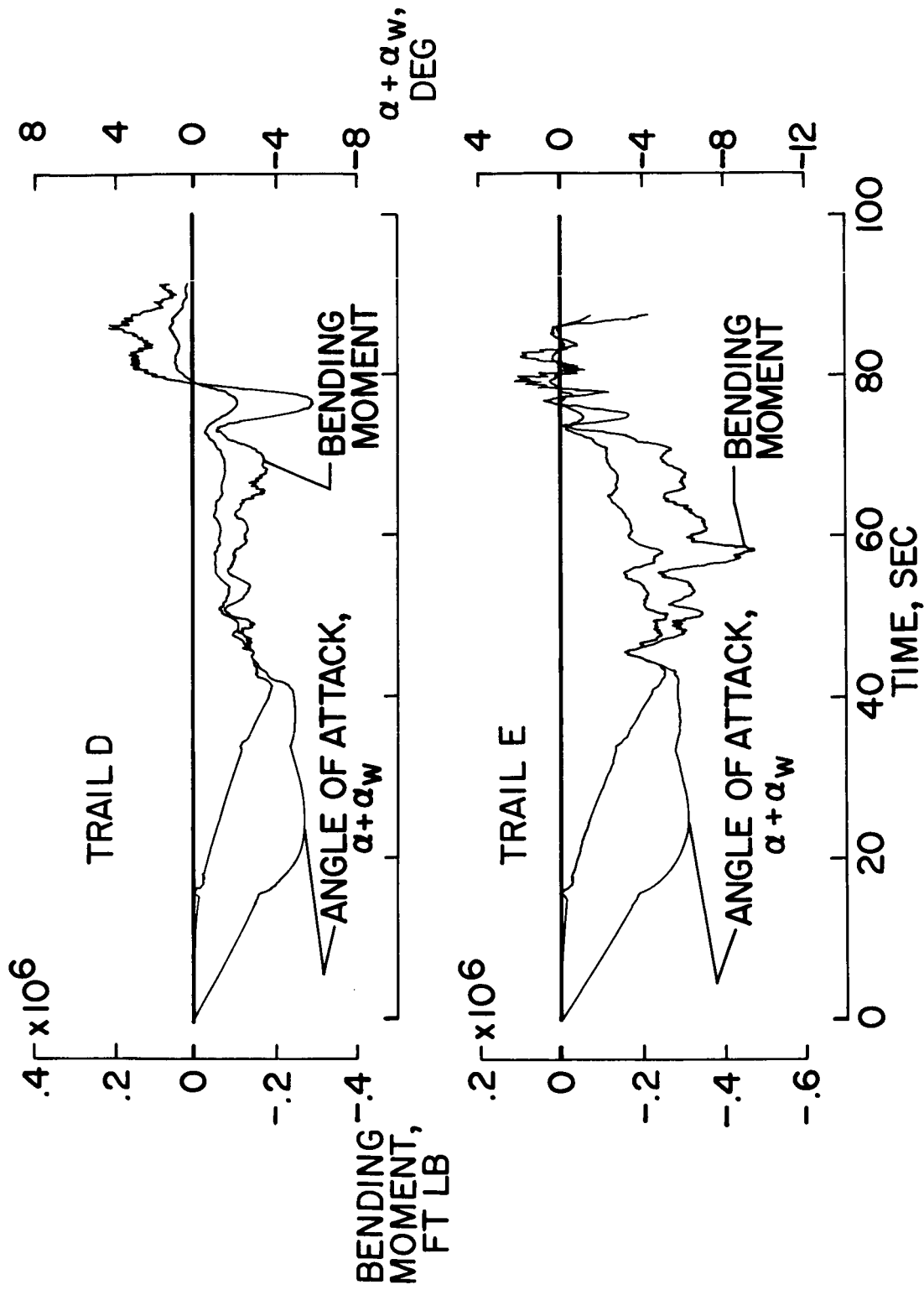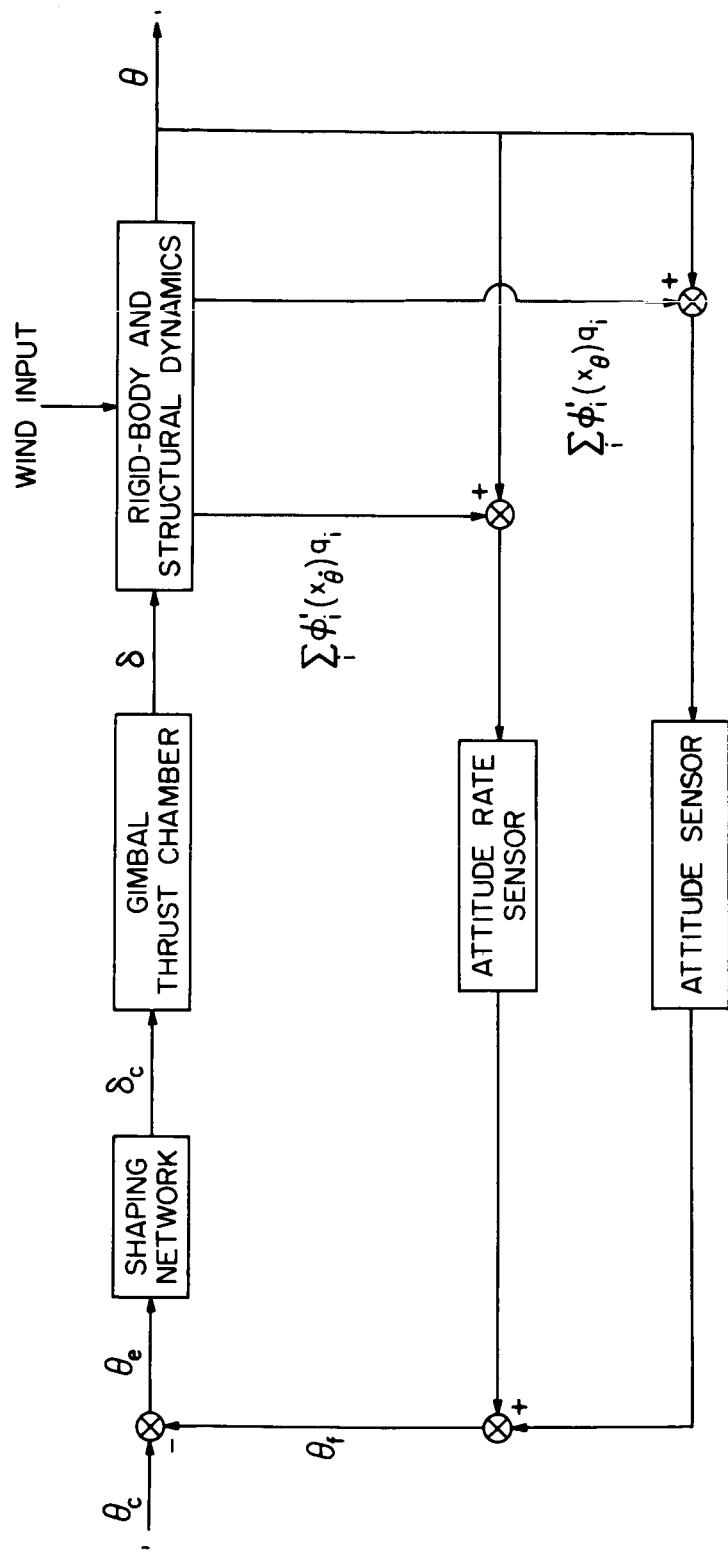
NASA

(b) Trails D and E.

Figure 8.- Continued.
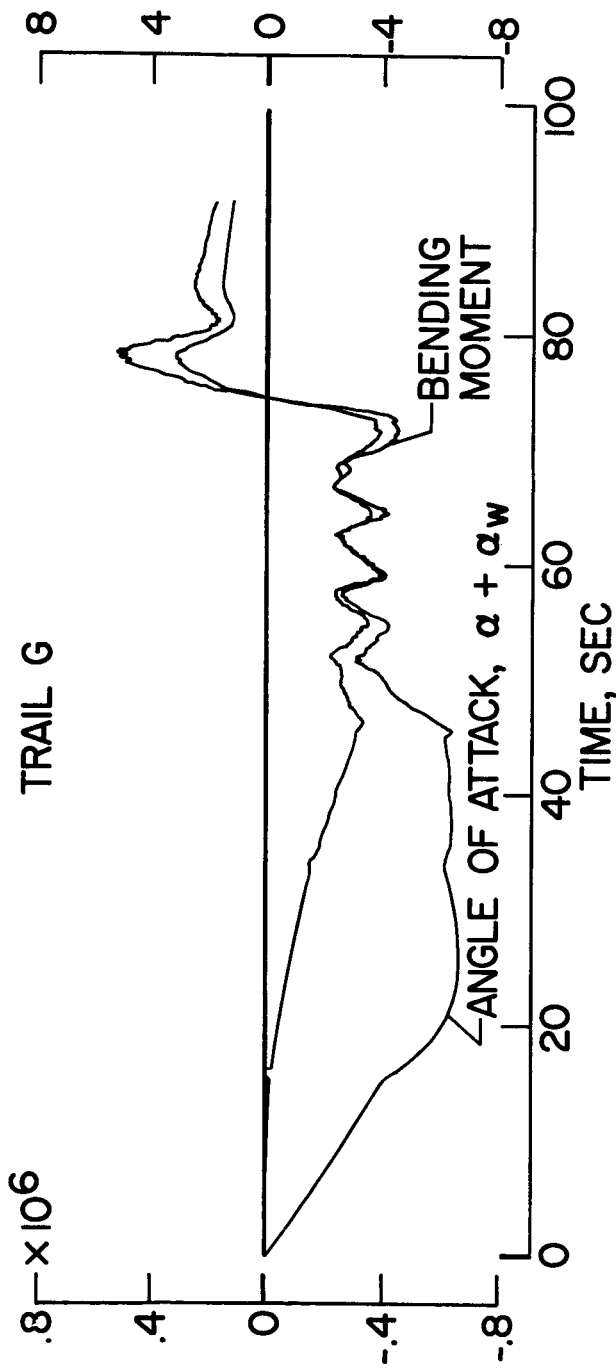
NASA

(c) Trails F and G.

Figure 8.- Concluded.

NASA

Figure 9.- Control-system block diagram.